Available online at www.sciencedirect.com
ScienceDirect
Computer Physics Communications 177 (2007) 110–113
Computer Physics Communications
www.elsevier.com/locate/cpc

Computational plasma nanoscience: Where plasma physics meets surface science

K. Ostrikov [a,*], I. Levchenko [a], S. Xu [b]

[a] *Plasma Nanoscience@Complex Systems, School of Physics, The University of Sydney, Sydney NSW 2006, Australia*
[b] *Plasma Sources and Applications Center, NIE, Nanyang Technological University, 631616 Singapore*

Available online 23 February 2007

Abstract

Multiscale hybrid simulations that bridge the nine-order-of-magnitude spatial gap between the macroscopic plasma nanotools and microscopic surface processes on nanostructured solids are described. Two specific examples of carbon nanotip-like and semiconductor quantum dot nanopatterns are considered. These simulations are instrumental in developing physical principles of nanoscale assembly processes on solid surfaces exposed to low-temperature plasmas.

Keywords: Multiscale hybrid simulations; Plasma; Building units; Nanoassembly; Surface processes

Plasma nanoscience is a new and rapidly emerging research area at the cutting edge of the physics of plasmas and gas discharges, surface science, nanoscience and nanotechnology, materials science and engineering, structural chemistry, and astrophysics [1]. It is commonly accepted that numerical simulations is a powerful tool to develop novel approaches for tailoring the plasma-grown building units (BUs) in various self-organization processes at nanoscales. Examples of applications of such approaches include but are not limited to plasma-aided nanofabrication of nanodevices, nanostructured films, nanoassemblies with intricate architecture and exotic properties, deposition of ordered nanoparticle arrays on nanopatterned solids, and origin and self-organization of dusty matter in the Universe [1,2]. In laboratory, the existing approaches for fabricating exotic nanostructures and functional nanomaterials are mostly process-specific and suffer from cost-inefficient "trial and error" practices. One of the reasons is that the ability to control, in the ionized gas phase, the generation, transport, deposition, and structural incorporation of the building units of such films and structures, still remains elusive. Here, we introduce the advanced multiscale numerical simulations of linked processes in the ionized gas phase and solid surfaces. This opens a way to manipulating BUs both in the plasma sheath and on solid surfaces, which still remains an essentially intractable problem at the multi-order-of-magnitude edge between the plasma physics and surface science. Here we describe how multiscale hybrid numerical simulations can be used to bridge the gap between the processes in the ionized gas phase and on solid surfaces thus giving an unprecedented possibility to control the parameters of plasma-grown nanostructures and their arrays by manipulating the delivery of BUs from the plasma and their redistribution on solid surfaces and eventual structural incorporation into the nanoassemblies (NAs) being grown.

Fig. 1 shows a typical plasma-aided nanofabrication environment, with the spatial scales and numerical models involved summarized in Table 1.

The modeling of BU creation in the plasma spans the spatial scales of ∼0.5 m (typical sizes of plasma reactors), whereas the scales involved in the modeling of surface self-organization processes are 7–9 orders of magnitude smaller. The BU delivery through the plasma sheath spans over ∼10 μm–10 mm, which is a typical sheath width in low-temperature processing plasmas. In Table 1, the following notations are used: L is a typical dimension of plasma reactors, λ_s is the plasma sheath width, l_p is the size of the simulation area on the surface, h_{NA} and l_{NA} are the NA sizes in vertical (in the z-direction) and horizontal (in the x–y plane) directions. Our research is focused on two main groups of selected NAs and their nanopatterns. Group I includes

* Corresponding author.
E-mail address: K.Ostrikov@physics.usyd.edu.au (K. Ostrikov).

0010-4655/$ – see front matter
doi:10.1016/j.cpc.2007.02.049

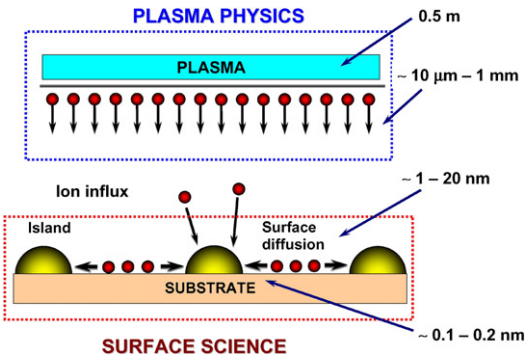

Fig. 1. Simulation environment.

Table 1
Numerical models and spatial scales in the multi-scale hybrid simulations. M1—BU generation, M2—BU delivery, M3—surface conditions, M4—pattern self-organization, and M5—NA growth

Module	Area	Scales
M1	Plasma bulk	$\lambda_s < z < L$
M2	Plasma sheath	$\lambda_s > z > h_{NA}$
M3	Surface	$x, y \sim l_p$
M4	Surface	$l_{NA} < x, y \sim l_p$
M5	Surface	$d_a < z \sim h_{NA}$
		$d_a < x, y \sim l_{NA}$

(mostly carbon-based) high-aspect ratio, nanotip-like structures of different dimensionality, such as nanotubes, nanoneedles and nanowires (1D), nanowall-like structures (2D), nanocones and nanopillars (3D) [3]. Group II includes semiconducting (e.g., SiC on Si/AlN, Si on Ge, AlN/AlInN on Si, etc.) quantum dot (QD) structures [5]. In most cases a detailed comparison of the results obtained by using plasma and charge-neutral fabrication routes (with the same main parameters) is made. Nanotip-like structures of Group I have $h_{NA} \sim 100$–900 nm and $l_{NA} \sim 10$–80 nm, whereas the sizes of nanodots of Group II is smaller ($h_{NA} \sim l_{NA} \sim 5$–$40$ nm). The choice of simulation geometries and other parameters is dictated by the relevant experimental results [1,4].

Positioning of individual NAs in nanopatterns reflects the most commonly used fabrication methods and patterning techniques. For example, nanotip-like structures are usually grown on catalyzed substrates pre-patterned via pattern transfer by using ordered templates, such as lithographic masks or porous materials. Hence, nanotip-like structures are positioned away from each other from tens of nanometers to several micrometers. On the other hand, tiny quantum dots are set in a pattern to reflect the commonly achievable surface coverage by the nanodots and some factors that can align or order them. Other process conditions, such as the surface temperature, DC substrate bias, working gas pressure, densities of plasma species, temperatures of electrons, ions, and neutrals, as well as other parameters, are taken as typical values of our most recent experiments [1,4].

Module M1 (Building unit generation) uses multi-fluid global plasma models and provides densities and energies of plasma species as functions of operating parameters [6]. It is adjusted to the modeling of $Ar + H_2 + CH_4/C_2H_2$ plasmas structures of Group I and $Ar + H_2$ (optional) $+ N_2$ (optional) plasma-assisted sputtering of Al, In, SiC, and Ge targets for the NAs of Group 2. This module generates fluxes of the plasma species at the sheath edge ($z = \lambda_s$) to be used in module M2.

Module M2 (BU delivery) uses Monte Carlo simulation to study the delivery of charged and neutral BUs from the plasma to the surface. It enables us to (i) compute the distribution of microscopic ion fluxes in the vicinity of and on nanostructured surfaces, including open surface areas (areas not covered by NAs) and lateral surfaces of individual nanostructures; (ii) relate the selective and targeted (e.g., to open surface areas or lateral surfaces) delivery of BUs to the plasma parameters such as the densities of the plasma species, electron temperature, etc.; and (iii) obtain (e.g., argon) ion fluxes required in M3 for computation of temperature and stress distributions on the surface. In this model, the species motion are traced from the plasma sheath edge to the nanopattern surface [3].

Module M3 (Surface conditions) contains the models of plasma-surface interactions (heat, momentum, and charge transfer) and specifies the effects of the plasma environment on the temperature, elastic stress and electric charge distribution on the growth surfaces. This module enables us to: (i) obtain the dependence of the surface temperature as a function of the ion flux; (ii) compute surface charge, charges on individual NAs and relate them to the plasma parameters. This module includes input from M2, builds on relevant processes in the plasma sheath and on solid surfaces [3,6] and provides the surface conditions required in M2, M4, and M5.

Module M4 (Pattern self-organization) describes the origin, development and self-organization of nanopatterns and contains two sub-modules [5]. The first sub-module M4-1 is used to model the nucleation of initial nuclei on surfaces subject to influx of species from the plasma and surface conditions (temperature, stress distribution, and electric charge) imported from M3. The positions and surface density of the initial growth islands strongly depend on the rates of collisions between adsorbed species, which are controlled by the BU influx from the plasma, surface temperature, and stress topography. This sub-module enables us to: (i) elucidate initial growth patterns; (ii) relate the size distribution and positioning of seed nuclei to the process parameters. It includes input from M2 and M3. M4-1 generates initial nucleation sites required in M4-2, M2, and M5. Sub-module M4-2 uses the advanced fluid-on-fluid technique [2], which is modified to describe migration of adsorbed adatoms and nanoisland growth and coalescence on plasma-exposed surfaces. This model of the nanopattern development in the plasma takes into account: (i) incoming BUs from the plasma; (ii) surface diffusion of adatoms; (iii) evaporation from the substrate surface and island surfaces; (iv) adatom attachment to the island surfaces; (v) island growth, displacement and coalescence [5]. This module enables us to: (i) describe density distributions of adsorbed species over nanostructured surfaces; (ii) evolution of developing nanopatterns subject to intake of building units from over the surface and directly from the plasma; (iii) take into account surface conditions (surface temperature and surface charge) computed in M3; (iv) relate the characteristics of NAs and nanopatterns to the plasma pa-

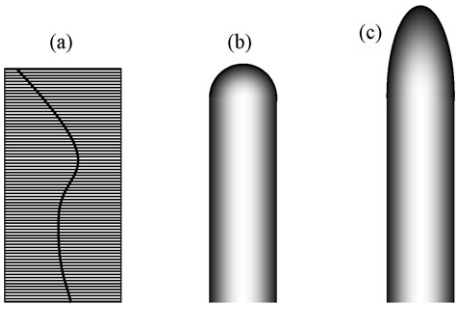

Fig. 2. Example of a carbon nanotip reshaped by a microscopic ion flux: (a) ion flux distribution over a lateral surface; (b) original nanotip; (c) reshaped nanotip.

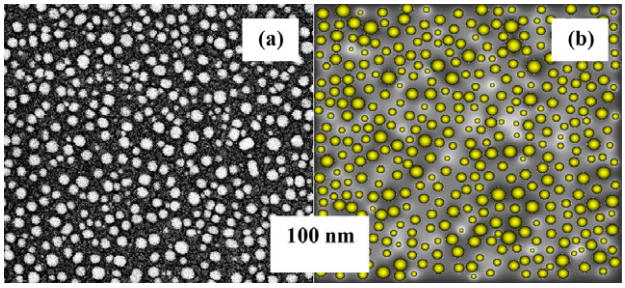

Fig. 3. Experimentally synthesized (a) [4] and computed (b) [5] surface morphology of SiC/Si(100) quantum dots synthesized by plasma-assisted RF magnetron sputtering of SiC in $Ar + H_2$ plasmas.

rameters. This sub-module includes input from M2, M3, and M5.

Module M5 (Nanoassembly growth) relates the growth kinetics of individual NAs from the initial nuclei to selective delivery of BUs (from over the surface and from the plasma) and surface conditions imported from M3 [3]. It enables us to follow the dependence of size and shape of individual nanostructures on the process conditions. This module is based on growth equations that relate the volume and shape of the structures to the incoming flux of BUs; it includes input from M2, M3, and M4.

We now show how our multiscale hybrid numerical simulation works in modeling the growth of two selected nanostructures from Groups I and II. In the first example, we consider carbon nanotip (CNs) microemitter structures, which should ideally feature high aspect ratios, vertical alignments, and uniformity in sizes (both in the x–y plane and the z-direction) across the entire nanopattern. We have shown that deposition of ionic BUs onto lateral surfaces of CNs can be effectively controlled by varying the plasma density, electron temperature, and DC bias of the substrate. For example, in low-density plasmas, ionic BUs deposit either onto open surface areas or on CNs closer to their bases. On the other hand, when the plasma is dense, the ions tend to land onto upper sections of the nanotip structures [3]. Assuming that the ions can directly incorporate into the NAs at the point of impact, we have demonstrated the possibility of deterministic shape control of the nanotips illustrated in Fig. 2. In this example, the plasma density is $n_p \sim 5 \times 10^{11}$ cm^{-3}, electron temperature $T_e = 1.5$ eV, bias potential $V_b = -30$ V, initial nanotip height $h_{NA} = 300$ nm and diameter $l_{NA} = 50$ nm. Nanotip shape can also be controlled during the growth process. Moreover, by using a plasma-based process, one can synthesize regular patterns of size-uniform high-aspect-ratio CNs, which turn out to be superior to similar nanopatterns synthesized by using a neutral gas with the same parameters. Specifically, the plasma-grown nanotips are taller and sharper, and more uniform within the entire simulation area, both in the surface plane and in vertical direction [3]. These results are also directly relevant to post-processing of quasi-1D structures, such as nanotubes, nanowires and nanoneedles. Indeed, relative positioning of such structures in a nanopatterns strongly affects the quality of their coating/functionalization by an ion flux from the plasma. The best results are achieved when the ion flux is deposited uniformly over the lateral surfaces and is not lost to open surface areas. This can be done at intermediate plasma densities and bias voltages and when the NAs are sufficiently spaced (by Δx) away from each other ($\Delta x \sim h_{NA}$).

The second example is related to Group II nanostructures, more specifically, SiC/Si(100) quantum dots grown by plasma-assisted RF magnetron sputtering of SiC targets in $Ar + H_2$ inductively coupled plasmas [5]. Fig. 3 shows the SEM micrograph of the experimentally synthesized (a) and a simulated growth pattern (b). This simulation is mostly based on modules M2–M4 and accounts for neutral and singly ionized Si, C, SiC BUs and involves two major stages. During the first stage, by using module M4-1, we computed the distribution of initial seed nuclei (ISNs, made of <25 atoms) subject to the incoming flux of BUs from the plasma (taken from the experiment [4]) at different surface temperatures. After optimization of size distributions, the ISNs were assigned random positions within the 1 μm × 1 μm pattern and their further growth was studied by using module M4-2. The final simulation pattern with the surface coverage ∼0.4, which is within reasonable accuracy recovers the experimentally achieved surface coverage [4], is shown in Fig. 3(b). In our simulations, we have also used more complex plasma chemistries, such as reactive nanocluster-generating plasmas [6]. The results of recent numerical simulation [5] of deposition of Ge/Si(100) quantum dot seed sub-monolayers from ionized and neutral germane GeH_4 gas show the advantages of the plasma route in controlled (∼1..3 × 10^{-4} monolayers) growth of ultra-small (containing 3..15 Ge atoms) seed nuclei suitable for the growth of uniform quantum dot patterns with a high surface coverage. It is remarkable that the proposed technique challenges the conventional Stranski–Krastanov growth mode, is applicable for a broader range of epitaxial systems, and is promising for deterministic synthesis of nanodevice-grade quantum dot arrays.

In summary, we have implemented a multi-scale, hybrid "macroscopic" model, which is capable to bridge the processes separated by spatial scales of nine orders of magnitude and normally considered by "3D" Plasma Physics and "2D" Surface Science, two seemingly unbridgeable areas of study. The model builds on the established, commonly used, well proven and justified principles and approaches of Surface Science to surface diffusion phenomena, island nucleation and growth [2]. We advanced these models by involving individual treatment of each NA (up to ∼10^3 in the pattern with each NA containing up to

∼1.5–2 million atoms) arranged on plasma-exposed surfaces. Owing to limitations of the present-day atomic-level *ab initio* models (e.g., in the number of atoms they can handle), our approach seems to be the most appropriate to describe nanopattern growth on plasma-exposed surfaces. Finally, the model is supported by numerous experimental and computational results [1,4] and it has an outstanding potential to bridge the "unbridgeable" Plasma Physics and Surface Science. Partial support from the ARC and ASTAR is acknowledged.

References

[1] K. Ostrikov, Rev. Mod. Phys. 77 (2005) 489.
[2] (a) F. Rosei, J. Phys. Cond. Matt. 16 (2004) S1373;
(b) S.V. Vladimirov, K. Ostrikov, Phys. Repts. 393 (2004) 175.
[3] (a) I. Levchenko, et al., J. Appl. Phys. 98 (2005) 064304;
(b) Appl. Phys. Lett. 89 (2006) 033109;
(c) E. Tam, I. Levchenko, K. Ostrikov, J. Appl. Phys. 100 (2006) 036104;
(d) I. Levchenko, K. Ostrikov, E. Tam, Appl. Phys. Lett. 89 (2006) 223108.
[4] (a) S. Xu, et al., Vacuum 80 (2006) 621;
(b) Z.L. Tsakadze, et al., Diam. Relat. Mater. 13 (2004) 1923;
(c) Z.L. Tsakadze, K. Ostrikov, S. Xu, Surf. Coat. Technol. 191 (2005) 49;
(d) K. Ostrikov, et al., Vacuum 80 (2006) 1126.
[5] (a) A. Rider, I. Levchenko, K. Ostrikov, J. Appl. Phys. 101 (2007) 044306;
(b) I. Levchenko, K. Ostrikov, SPIE Proc. "Microelectronics, MEMS and Nanotechnology" 6039 (2006) 60390L;
(c) C. Mirpuri, et al., J. Appl. Phys. 101 (2007) 024312.
[6] (a) I.B. Denysenko, et al., J. Appl. Phys. 95 (2004) 2713;
(b) I.B. Denysenko, et al., J. Appl. Phys. 94 (2003) 6097;
(c) K. Ostrikov, et al., Phys. Rev. E 67 (2003) 056408;
(d) K. Ostrikov, et al., Plasma Proc. Polym. 4 (2007) 27;
(e) K. Ostrikov, et al., Phys. Rev. E 61 (2000) 782;
(f) K. Ostrikov, M.Y. Yu, IEEE Trans. Plasma Sci. 26 (1998) 100.